Anisotropic Processing of Image Structures for Adventitia Detection in Intravascular Ultrasound Images

AH Hernandez[1], DG Gil[1], PR Radeva[1], EN Nofrerias[2]

[1]Computer Vision Center, Universitat Autonoma de Barcelona, Bellaterra, Barcelona, Spain
[2] Hospital Universitari Germans Trias i Pujol, Badalona, Spain

Abstract

The adventitia layer appears as a weak edge in IVUS images with a non-uniform grey level, which difficulties its detection. In order to enhance edges, we apply an anisotropic filter that homogenizes the grey level along the image significant structures (ridges, valleys and edges). A standard edge detector applied to the filtered image yields a set of candidate points prone to be unconnected. The final model is obtained by interpolating the former line segments along the tangent direction to the level curves of the filtered image with an anisotropic contour closing technique based on functional extension principles.

1. Introduction

IVUS clinical interest feeds development of image processing techniques addressing detection of arterial structures [1], [2], [3], [4], such as intima segmentation or plaque characterization. However, although adventitia detection is crucial for a reliable plaque quantification, the topic has been hardly approached [5], [6]. In this paper, we present a novel method for adventitia segmentation based on local orientation of image structures.

We split the problem of adventitia detection in two stages: extraction of points laying on the adventitia and recovery of a closed model of such points. In both steps the restricted anisotropic operators introduced in [7], [8] play a central role. Anisotropic diffusion bases [9] on a heat propagation model on a surface/medium where heat does not distribute equally in all directions, but according to the ellipse defining the diffusion tensor. A common trend in filtering algorithms [9], [10], [11] is to align the diffusion tensor major axis along a particular image structure (edges, valleys, ridges, vessels). In this fashion, the resulting anisotropic diffusion delays blurring of the gray level changes that define such image feature. However, because gray values spread on the whole image plane one still needs to seek for the time/iteration/scale achieving the best compromise between noise removing and preserving significant image features. In order to ensure that image structures will be preserved we restrict diffusion to a vector field smoothly approaching image level sets tangent space. The associated image filtering operator homogenizes gray levels and response of image structures defined by contrast changes (such as edges, ridges, valleys) and, at the same time, smoothes noisy areas.

We select adventitia candidate points by means of the negative edges of minimum radius extracted from IVUS images in polar coordinates. Edges are computed with a first derivative of a Gaussian over images filtered with a Restricted Anisotropic Diffusion (RAD) and longitudinal cuts serve to remove the intima layer. The former two steps ensure that the final set of connected components, though uncompleted, lay on the adventitia. In order to interpolate curve segments, we use restricted anisotropic operators to extend a mask function of the unconnected set of points. By changing the boundary conditions of the diffusion process to Dirichlet, so that the evolving function is forced to take the values of the initial mask at the curve segments to be joined, we model our Anisotropic Contour Closing (ACC) [8]. The process yields an implicit level sets model of the adventitia that captures curvatures as it bases on the image local orientation. For the sake of a representation as compact as possible we use classic B-snakes [12] for the final explicit parametrization.

Our strategy has been validated with in-vivo sequences previously segmented by an expert. The statistics on the maximum and mean positioning error show that our segmentation is optimal in those cases that the adventitia is thoroughly described as an edge. Moreover, our reconstruction of the adventitia is more accurate than other interpolating algorithms that produce piece-wise linear models (e.g. geodesic snakes).

2. Restricted anisotropic operators

Most filtering techniques based on image gray level modification [9] use the heat diffusion equation:

$$u_t(x, y, t) = \mathrm{div}(J \nabla u)$$

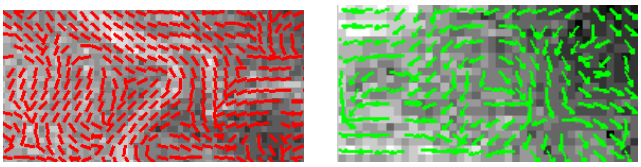

(a) (b)

Figure 1. Vector field at noisy (a) and regular (b) areas

The time dependant function u is the family of smoothed images and J is a 2-dimensional metric (i.e. an ellipse) that locally describes the way gray levels re distribute. The diffusion tensor J is thoroughly described by means of its eigenvectors (ξ, $\eta = \xi^{\perp}$) and eigenvalues (λ_1, λ_2). If the latter are strictly positive, gray values spread on the whole image plane and the family u converges to a constant image. On the other side if we degenerate J (i.e. we admit null eigenvalues), then the final image [7] is a collection of curves of uniform gray level. A suitable choice of the eigenvector of positive eigenvalue leads to our:

Restricted Anisotropic Diffusion (RAD)

Let us consider a metric $\tilde{J}$ with eigenvalues $\lambda_1 = 1$ and $\lambda_2 = 0$, and ξ the eigenvector of minimum eigenvalue of the Structure Tensor. The Restricted Heat Diffusion we suggest is given by:

$$u_t = \mathrm{div}(\tilde{J}\nabla u) \quad \text{with} \quad u(x, y, 0) = u_0(x, y) \qquad (1)$$

for u_0 the image to be de-noised. Notice that in a band around the image significant structures (fig.1(a)), ξ yields a smooth closed model of their tangent space. Meanwhile at noisy areas (fig.1(b)), it is a random vector that locally generates the whole 2 dimensional space. The result is that gray levels homogenize along image regular level sets and solutions to (1) converge to a smooth image that enhances the main features of the original image, in the sense that their response to standard detectors is uniform. Figure 2 shows the improvement of the ridges in an angiography. Background spurious ridges due to noise in fig.2(a) have been removed, in a similar fashion a gaussian smoothing would do, while ridges corresponding to the vessel are closed curves in the RAD image of fig.2(b).

Still heat diffusion has another mathematical and physical use hardly exploited in image analysis. Heat diffusion has the property of smoothly extending a function defined on a curve in the plane, provided that boundary conditions are changed to Dirichlet [13]. By using restricted heat operators this property can be used to complete unconnected contours [8] as follows.

Anisotropic Contour Closing (ACC)

Let γ be the set of points to connect, χ_γ its characteristic function (a mask) and define $\tilde{J}$ as in RAD, then the

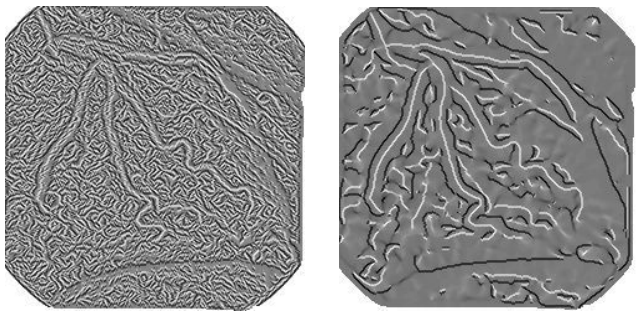

(a) (b)

Figure 2. Ridge enhancement: original (a) and RAD (b)

extension process given by:

$$u_t = \mathrm{div}(\tilde{J}\nabla u) \quad \text{with} \quad u_{|\gamma} = u_0 \qquad (2)$$

converges to a close model of γ. Intuitively, we are integrating the vector field ξ, that is, we are interpolating the unconnected curve segments along it. First, notice that by using a restricted heat equation (2) we ensure convergence to a closed model of the unconnected curve γ, whatever its concavity is. Second, because ξ takes into account image level sets geometry, ACC closure is more accurate than other interpolating techniques (such as geodesic snakes) which, at most, yield piece-wise linear models, provided they succeed in converging to the uncompleted curve segments.

Let us now describe how the former techniques can combine into an adventitia modeling algorithm.

2.1. The detection strategy

Following [7] we will approach adventitia segmentation by selecting first a set of candidate points and, afterwards, giving a close model as compact as possible.

1. Finding points on the adventitia layer

In an IVUS plane, the adventitia is a circular line/structure, which motivates working in polar coordinates. In order to reduce the impact of heart movement and eccentricity, we place the origin at the geometric mass center of a set of points roughly lying on that vessel structure. In such coordinate system and provided we consider positive orientation, the adventitia corresponds to negative vertical edges. Further, edges will be extracted from RAD filtered images, so that noise impact is reduced and edge response strengthen. Still, sparse fake responses and points on the intima layer, which is also characterized as a negative edge, are detected. For a selection of true adventitia points we will consider that an edge connected component is on the right vessel layer if it corresponds to an edge of minimum radius in a longitudinal cut. Snakes are used to ensure that

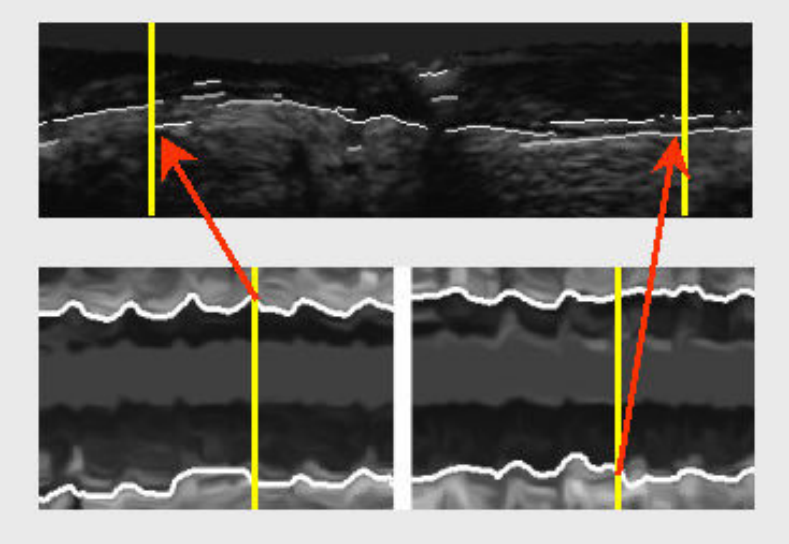

Figure 3. Selection of adventitia candidate points

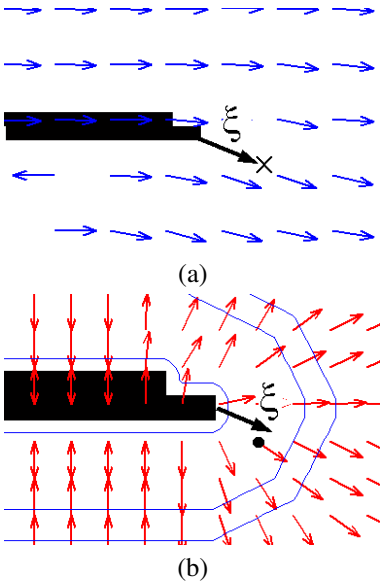

Figure 4. ACC quick integration

we deal with completed edges enclosing all frames. The whole selecting stage is summarized in fig.3.

2. Computing a closed model

To fill-in gaps within candidate segments we will first compute a closed model in implicit level sets form and then use a Bspline snake to produce a compact model of the adventitia. In order to obtain models as accurate as possible we will use ACC with the structure Tensor compute over the edge map used in the previous step. For the sake of a computational cost as small as possible, we use the following quick algorithm for solving equation (2). First recall that the final image yielded by ACC is a mask (i.e. 1's and 0's) of the closed curve and that the whole process might be regarded as integrating the field ξ. Then, since the divergence term develops as:

$$\mathrm{div}(\tilde{J}\nabla u) = \mathrm{div}(\langle \xi, \nabla u \rangle \xi)$$

we have that, for each border point of a segment, the next pixel to be set to 1 is the neighbor in the direction ξ (cross in fig.4(a)). Such pixel achieves the maximum correlation between ξ and the gradient of the distance map to the uncomplete curve (dot in fig.4(b)). In this manner the whole closing process is of the order of the gap (pixel) size. Figure 4 illustrates the grounds of the algorithm: the vector to be integrated is shown in fig.4(a) and the distance map gradient used to compute ACC in fig.4(b).

3. Results

Final snakes modelling the adventitia of the images in the first row are depicted in the second row of fig.5. Validation of the method has been based on the following:

3.1. Assessment protocol

A total number of 1000 frames extracted from 5 different patients (200 per sequence) have been analyzed. The measures used to quantify accuracy of the automated detections are the mean and maximum positioning error and area differences between our model and a manual segmentation. The sequences have been manually segmented by 3 different physicians every 10 frames in order to analyze inter-observer variation.

3.2. Statistical measurements

The variation for distances (in mm) and percentage of area difference for each of the patients, as well as, total numbers are summarized in table 1. The global mean distance error is under 0.3 mm., which brings our adventitia detection close to intima segmentation algorithms [2]. Because final snake models do not take into account any continuity along the sequence, there are some isolated miss segmentations that increase maximum errors as well as area differences. Patients 1,2 and 4 present average errors (a mean distance error of 0.23 ± 0.09) close to inter-observer variability. Subject 3 bad statistics result from basing adventitia characterization exclusively in edges, since the sequence presents a structure (bright area in upper left part of the image in fig.5(c)) with similar changes in image gray values. Meanwhile, high deviations in the last patient are result of a low quality in images, as the large inter-observer error (it is the worst with a discrepancy in layer location up to $0.81mm$).

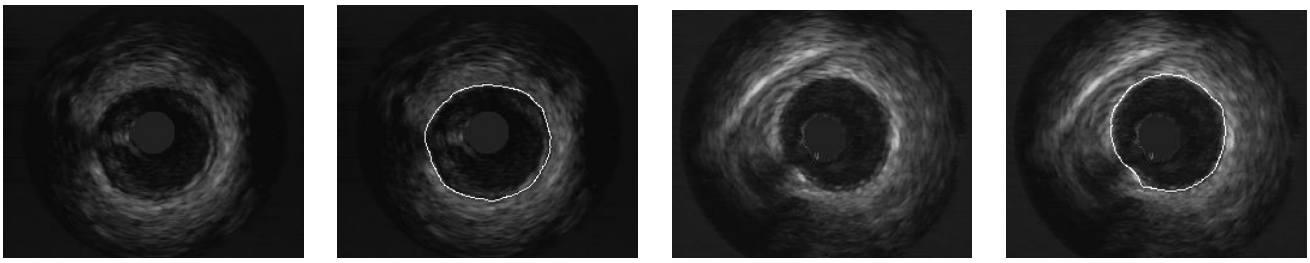

(a) (b) (c) (d)

Figure 5. Adventitia Models (b), (d) of the original (a), (c)

Table 1. Statistical Error

	Subject 1	Subject 2	Subject 3	Subject 4	Subject 5	Global
INT-OBS. Max. Dist. **(mm)**	0.3 ± 0.11	0.46 ± 0.17	0.32 ± 0.13	0.41 ± 0.14	0.55 ± 0.26	0.42 ± 0.2
INT-OBS. Mean Dist. **(mm)**	0.12 ± 0.02	0.19 ± 0.06	0.15 ± 0.05	0.17 ± 0.05	0.24 ± 0.12	0.18 ± 0.08
INT-OBS. Area Dif. **(%)**	4.47 ± 1.04	6.34 ± 2.45	6.29 ± 2.87	6.62 ± 2.66	9.8 ± 5.3	7 ± 3.7
AUT. Max. Dist. **(mm)**	0.69 ± 0.28	0.67 ± 0.27	0.75 ± 0.4	0.79 ± 0.65	1.0 ± 0.62	0.80 ± 0.52
AUT. Mean Dist. **(mm)**	0.25 ± 0.08	0.23 ± 0.04	0.26 ± 0.09	0.27 ± 0.12	0.33 ± 0.16	0.27 ± 0.12
AUT. Area Dif. **(%)**	9.91 ± 4.02	7.74 ± 1.72	12.35 ± 3.95	10.79 ± 4.34	13.76 ± 6.84	11.16 ± 5.08

4. Discussion and conclusions

The detection of the adventitia layer presented in this paper is a new trend in medical imaging with a straightforward clinical application to plaque area and vessel diameter measurements. The fact that the segmenting strategy combines simple standard techniques increases its efficiency and applicability. A key point is the use of restricted anisotropic operators, which represents an improvement in quality of filtered images and accuracy of final models. Since the modelling algorithm exclusively relies on the features used to characterize the adventitia, our future research will focus on looking for a better set of descriptors of the structure.

Acknowledgements

References

[1] McInerney T, Tezopoulos D. Deformable models in medical images analyis: a survey. Medical Image Analysis 1996;1:91–108.

[2] Zhang X, Sonka M. Tissue characterization in intravascular ultrasound images. IEEE Trans on Medical Imaging 1998; 17:889–899.

[3] Pujol O, Radeva P. Supervised Texture classification for Intravascular Tisue Characterization, Handbook of Medical Imaging. Kluwer Academic/Plenum Publishers, 2004.

[4] Rosales M, Radeva P, Mauri F. Simulation model of intravascular ultrasound. In MICCAI'04; .

[5] Klingensmith J, Shekhar R, Vince D. Evaluation of three-dimensional segmentation algorithms for the identification of luminal and medial-adventitial borders in intravascular ultrasound. IEEE Trans on Medical Imaging 2000;19.

[6] Shekar R, Cothren R, Vince D, Chandra D, Thomas J, Cornhill J. Evaluation of three-dimensional segmentation algorithms for the identification of luminal and medial-adventitial borders in intravascular ultrasound. Computerized Med Imag and Graphics 1999;23:299–309.

[7] Gil D. Geometric Differential Operators for Shape Modelling. Ph.D. thesis, Universitat Autonoma de Barcelona, 2004.

[8] Gil D, Radeva P, Vilariño F. Anisotropic contour completion. In ICIP'03; .

[9] Weickert J. A Review of Nonlinear Diffusion Filtering, Scale-Space Theory in Computer Vision. Lecture Notes in Comp. Science, Springer-Verlag, 1997.

[10] Carmona R, Zhong S. Adaptative smoothing respecting feature directions. IEEE Trans Image Proc 1998;7.

[11] Cañero C, Radeva P. Vesselness enhancement diffusion. Patt Recog Letters 2003;24:3141–3151.

[12] Kass M, Witkin A, Terzopoulos D. Snakes:active contour models. Int Journal of Computer Vision 1987;1.

[13] Evans L. Partial Differential Equations. Berkeley Math. Lect. Notes, 1993.

Address for correspondence:

Aura Hernández, Debora Gil

Centre de Visió per Computador, Edifici O, Campus UAB, 08193 Bellaterra, Barcelona, Spain.

aura,debora@cvc.uab.es